Fatma Cansu Yücel, Fabian Habicht, Myles D. Bohon, Christian Oliver Paschereit

Autoignition in stratified mixtures for pressure gain combustion

Autoignition in Stratified Mixtures for Pressure Gain Combustion

Fatma Cansu Yücel[a,*], Fabian Habicht[a], Myles Bohon[a], Christian Oliver Paschereit[a]

[a]*Technical University of Berlin, Institute of Fluid Dynamics and Technical Acoustics, Müller-Breslau-Strasse 8, Berlin and 10623, Germany*

Abstract

The reliable generation of quasi-homogeneous autoignition inside a combustor fed by a continuous air flow would represent a milestone in realizing pressure gain combustion in gas turbines. In this work, the ignition distribution inside a stratified fuel–air mixture is analyzed. The ability of precise and reproducible injection of a desired fuel profile inside a convecting air flow is verified by applying tunable diode laser absorption spectroscopy in non-reacting measurements. High-speed, static pressure sensors and ionization probes allow for simultaneous detection of the flame and pressure rise at several axial positions in reactive measurements with dimethyl ether as fuel. A second, exchangeable combustion tube enables optical observation of OH^* intensity in combination with pressure measurements. Experiments with three arbitrary fuel profiles show a set of ignition distributions that vary in shape, homogeneity, and the number of simultaneous autoignition events. Although the measurements show notable variation, a significant and reproducible influence of the fuel injection on the ignition distribution is observed. Results show that uniform autoignition leads to a coupling of the reaction front with the pressure rise and, therefore, induces a greater aerodynamic constraint than non-uniform ignition distributions, which are dominated by propagating deflagration fronts.

Keywords:
homogeneous autoignition, fuel stratification, pressure gain combustion, shockless explosion combustor

*Corresponding author:
Email address: `f.yuecel@tu-berlin.de`
(Fatma Cansu Yücel)

1. Introduction

Replacing the conventional isobaric combustion of the gas turbine cycle by pressure gain combustion is a promising concept to achieve improvements in cycle efficiency. Different approaches have been investigated, such as pulse detonation combustion (PDC) [1] and rotation detonation combustion (RDC) [2]. Both concepts utilize propagating detonation wave(s), the high temperatures and pressures of which present significant engineering challenges. An alternative approach, called shockless explosion combustion (SEC) [3], overcomes these challenges by using quasi-homogeneous autoignition to achieve approximately constant volume combustion without the presence of a detonation wave or mechanical constraints.

Homogeneous autoignition occurring in well mixed combustible mixtures was originally referred to as thermal explosion by Zel'dovich [4] as a concept of spontaneous flames, leading to an increase in pressure similar to constant volume combustion. However, non-uniformities in the mixture, such as variations in temperature, pressure or equivalence ratio, can cause deviations in ignition delay time and result in a propagating autoignition front instead. The propagation velocity of this autoignition front u_{ai} is inversely proportional to the spatial gradient of the ignition delay time τ_{ai}. Assuming constant temperature T and pressure p across the mixture, the ignition delay time τ_{ai} is a function of the equivalence ratio φ such that u_{ai} can be expressed as:

$$u_{\mathrm{ai}} = \left(\frac{\partial \tau_{\mathrm{ai}}}{\partial x}\right)^{-1} = \left(\frac{\partial \tau_{\mathrm{ai}}}{\partial \varphi}\frac{\partial \varphi}{\partial x}\right)^{-1}. \tag{1}$$

Comparing u_{ai} to the speed of sound a leads to the dimensionless parameter ξ, where

$$\xi = \frac{a}{u_{\mathrm{ai}}} = a\,\frac{\partial \tau_{\mathrm{ai}}}{\partial \varphi}\frac{\partial \varphi}{\partial x}. \tag{2}$$

This allows for the description of different combustion modes [4, 5]. A subsonic propagation of the reaction front occurs when $\xi > 1$. For $\xi = 1$ the propagation velocity of the autoignition front is equal to the speed of sound, allowing amplification by coupling and enabling deflagration-to-detonation transition (DDT). The ideal process of thermal explosion, which occurs for $\xi = 0$, is not practical in experiments due to unavoidable perturbations of the initial conditions and mixture inhomogeneity, leading to gradients in reactivity. However, $\xi < 1$ results in a quasi-homogeneous autoignition leading to an approximate constant volume combustion while avoiding DDT. Similar behavior in pressure rise

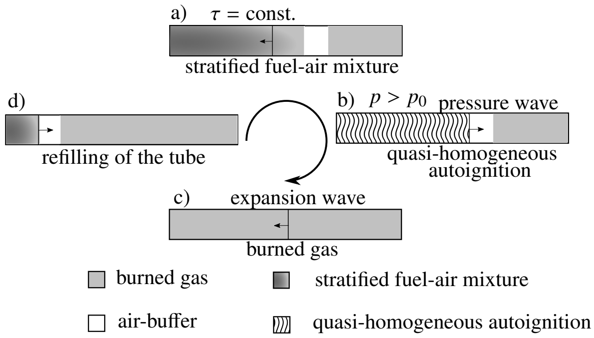

Figure 1: Sketch of the single tube SEC test rig

can be observed in the case of multiple separate ignition sources that ignite quasi-simultaneously [6]. This regime of quasi-homogeneous autoignition and/or many distributed ignition points is the objective for the implementation of SEC.

Along these principles, the realization of homogeneous charge compression ignition (HCCI) has been investigated intensively in the past [7]. Preventing engine knock is a major challenge in HCCI and has been addressed by applying different methods, such as modification of oxidizer and fuel properties, equivalence ratio, exhaust gas recirculation, or engine parameters [8]. However, the implementation of this concept in a gas turbine cycle for pressure gain combustion is a new approach.

The SEC is based on a periodic combustion process as sketched in Fig. 1. The cycle begins with a stratified, autoignitable fuel–air mixture throughout the combustor (Fig. 1a). This stratification has been tailored to compensate for the gradient in residence time, resulting in a quasi-homogeneous autoignition (Fig. 1b). The pressure rise during combustion induces a pressure wave propagating downstream which is reflected as an expansion wave when reaching the acoustically open combustor outlet (Fig. 1c). When this wave reaches the combustor inlet, the refilling process begins (Fig. 1d) and the cycle restarts.

The objective of this work is to investigate the ignition processes within a stratified fuel–air mixture. First, the ability of injecting a defined mixture profile in a convecting air flow is analyzed. Subsequently, the homogeneity of measured autoignition times and pressure rise as a function of the fuel stratification are examined. Finally, the processes of autoignition homogeneity, flame propagation, and process variability are studied in high-speed images of OH^* chemiluminescence.

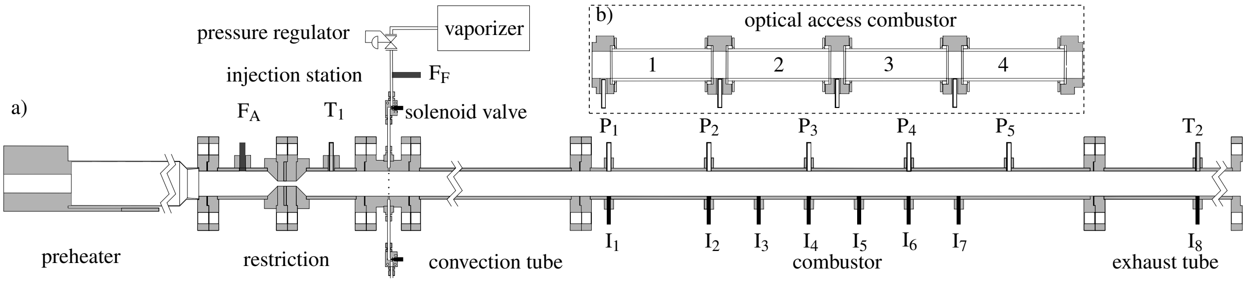

Figure 2: Sketch of the test rig. Sensors: low-speed, static pressure sensors (F_A, F_F), thermocouples (T_1, T_2), high-speed, static pressure sensors (P_1–P_5), ionization probes (I_1–I_8). The inset subfigure b) shows the exchangeable version of the combustor tube with optical access.

2. Experimental Setup and Measurement Procedure

A sketch of the test rig for the experimental investigation of autoignition of an axially stratified fuel–air mixture in a convecting flow is shown in Fig. 2. The test rig is composed of several sections, including reactant injection, convection (0.5 m), combustor (0.5 m), and exhaust (1 m) sections. All sections have an inner diameter of 40 mm. The rig was originally designed by Bobusch et al. [3, 9] and later used by Reichel et al. [10]. However, in these works, reproducibility was limited and consistent homogeneous autoignition was difficult to achieve. The control of the injection process has since been improved by Yücel et al. [11].

In the reacting cases, a preheater is used to raise the temperature of the constant air flow to 1023 K measured at T_1. Downstream of the preheater, the air flow is forced through a restriction in order to prevent backflow of hot gases into the preheater due to ignition. Fuel is injected via ten radial ports with 1 mm diameter each, which are individually controlled by high-speed solenoid valves (Staiger VA 204-716). A dome-loaded pressure regulator (Swagelok RD6) is installed upstream of the injection station to control the fuel supply pressure. Two static pressure sensors F_A and F_F (Festo SPTW) are installed to monitor the air and fuel supply pressures. The fuel injection duration is $\Delta t_{inj} = 50\,\mathrm{ms}$, and is divided into ten time windows, each with a length of 5 ms. The number of open valves is individually set for each time window defining the injected fuel profile.

The modular setup allows for exchanging the stainless steel combustor for a quartz tube (Fig. 2b) in order to achieve optical access. This configuration is used for fuel concentration measurements and OH* chemiluminescence imaging of the ignition distribution.

2.1. Fuel Concentration Measurements

Fuel concentration measurements using near-infrared tunable diode laser absorption spectroscopy (TDLAS) are conducted as proposed by Li et al. [12]. These measurements are used to validate the control of the injection geometry to achieve a desired mixture profile within a defined time frame. This technique has been used previously for time-resolved fuel concentration measurements in a similar configuration [10, 13]. While the combustion experiments in this work are conducted with dimethyl ether (DME) as fuel, the concentration measurements are done with methane to match the absorption features around a wavelength of 1654 nm utilizing the available laser. In the scope of this work, we expect the variation in the injected mixture fraction profile to be primarily controlled by turbulent diffusion and mixing. Since turbulent fluctuations scale with the Reynolds number, it is considered as the dominant mixing parameter rather than molecular diffusion (which is of the same order for both fuels). However, when comparing the Reynolds numbers for the non-reacting (approx. 48000) to reacting (approx. 6000) cases, it is expected that the non-reacting cases will exhibit much greater turbulent diffusion and a blurring of the mixture profile. Lastly, the residence time is kept constant for all measurements by matching the flow velocities, allowing an equal amount of time to diffuse. Considering this, it is reasonable to conclude that for the reacting cases the resulting gradients are steeper than TDLAS measurements reveal. While this prevents quantifying the exact local equivalence ratio for the reacting DME cases, it does allow for a qualitative measure of the reproducibility and accuracy of the injection scheme.

2.2. Reactive Measurements

For reactive measurements, the initial temperature is monitored via two Type-K thermocouples. Five water-cooled, high-speed pressure sensors are installed in the combustor with a distance of 100 mm to record the static pressure variation. The flame is detected via 8 ionization probes that are mounted in the combustor and the exhaust tube. Figure 2 shows the naming convention for each sensor.

The temperature at the injection station remains constant during the measurements. At the beginning of each measurement, a gradient in wall temperature of about 50 K between sensors T_1 and T_2 is observed. Heating during the run increases T_2 by approximately 50 K. However, the measurement data show no correlation between the ignition time throughout the measurement region and the measured wall temperature. Therefore, it is reasonable to assume the impact of the transient wall temperature on the ignition process to be negligible.

DME is used as fuel resulting in ignition times in the range of 60 ms to 80 ms for the applied conditions (p=1 atm, T=1023 K and $1 \leq \varphi \leq 2$). This assures autoignition of the convecting mixture inside the combustor. The fuel supply pressure is F_F = 5.7 bar and the equivalence ratio is controllable from $\varphi = 0$ (all valves closed) to $\varphi = 2$ (ten valves open). The average fuel mass flow rate was measured under steady state conditions using a Coriolis mass flow meter. To assure a gaseous state, the fuel is vaporized and guided through a heated pipe (330 K) before injection.

The ignition behavior of DME is characterized by a negative temperature coefficient (NTC) region, which is studied in more detail by Burke et al. under high pressure conditions [14]. However, calculating the relevant ignition delay times with Cantera [15] for a zero-dimensional constant volume reactor using the mechanism AramchoMech2.0 that has been validated for DME-kinetics in previous works, reveal that all tests were conducted outside the NTC region of DME. Operating in the NTC region of DME would require accounting for additional non-linear behavior of DME autoignition, and is therefore avoided.

The optically accessible section is composed of a series of four quartz tubes, each 120 mm long, supported by stainless steel flanges fitted with one pressure sensor each. An optical band-pass filter (CWL = 310 nm, FWHM = 10 nm), an intensifier (Lambert Instruments HiCATT) and a high-speed camera (Photron Fastcam SA-Z) are used to detect the reaction zones by light emission of OH* intensity. The recorded high-speed images allow for observation of the ignition distribution at 87500 fps and a spatial resolution of 2.7 px/mm.

3. Results and Discussion

The results will be broken into two sections. First, the control of the fuel injection profile will be investigated, and three example contours will be discussed. The second section will then examine the autoignition characteristics of these profiles, focusing on the pressure rise (as representing aerodynamic confinement) and correlate the variation in pressure rise with direct observations of the homogeneity of autoignition.

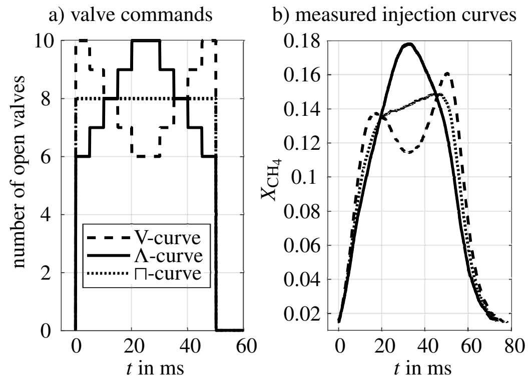

Figure 3: Injection curve commands for V-, Λ- and ⊓-curve (a) and measured methane concentration 50 mm downstream of the combustor inlet averaged over 150 cycles (b).

3.1. Fuel Injection

The mass flow rates of fuel and air are set to match the mixture bulk flow velocity for reacting experiments (u_{bulk} = 18 m/s). Each control sequence is injected for 150 cycles with an operating frequency of 5 Hz. Three different injection profiles are investigated at ambient pressure and temperature: (i) Λ-curve, (ii) V-curve and (iii) ⊓-curve. The control sequences and the respective TDLAS measured, cycle averaged fuel concentration for the three trajectories are shown in Fig. 3.

The averaged results clearly show the capability of replicating a desired fuel profile within the given time span Δt_{inj}. The measured fuel profiles of individual cycles show a standard deviation (std) of less than 5 % throughout the injection. There is a clear smoothing effect, especially in the regions of high gradient. This is expected and can be attributed to two effects: (i) turbulent diffusion and (ii) shear layer effects. Diffusion will smooth the sharp features of the injection profile (beginning and end of injection period). The shear layer effect near the wall causes a variation in the velocity profile through the tube and induces a spatial distortion of the injection profile. This phenomenon can only be measured as an integrated value across the tube through the line-of-sight measurement. It is also important to mention that due to inertia of the valves, there is a hysteresis to the valve response when opening and closing, the effects of which are difficult to account. Currently, there is no way to avoid these effects, and must instead be accounted for when interpreting the reacting results.

For reacting tests, it is important to maintain a constant cycle-averaged fuel flow rate, otherwise differences in pressure rise might occur due to variations in total heat release. For this, the total valve-open time

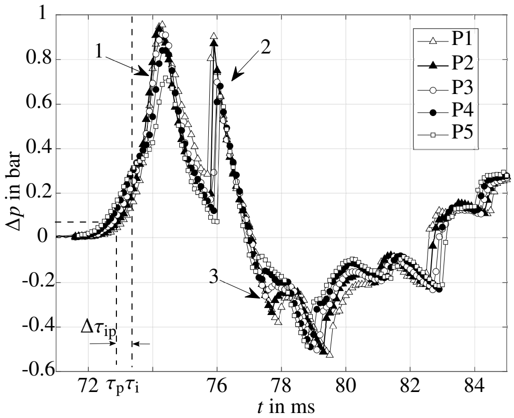

Figure 4: An example pressure history during ignition event for pressure sensors P_1 to P_5 resulting from the injection of the Λ-curve.

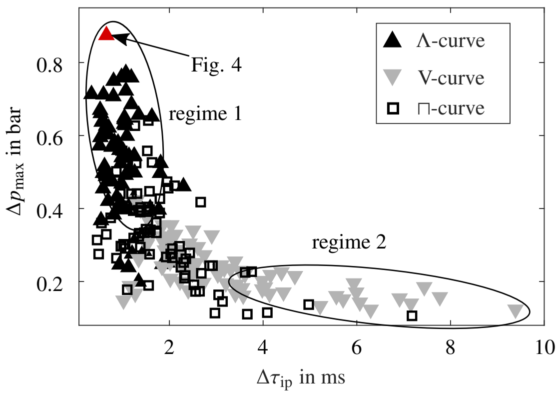

Figure 5: Pressure amplitude over delay $\Delta\tau_{ip}$ between autoignition and pressure rise for each cycle.

is maintained constant through the injection period and averaged to eight open valves. This corresponds to an average equivalence ratio of the fuel–air mixture of $\varphi = 1.6$. The variation of the integrated area of the measured fuel concentrations shown in Fig. 3b is within the measurement uncertainty. Therefore, the reactant injection profile can be maintained and controlled with reasonable certainty.

3.2. Autoignition Control

For the following investigations, the air mass flow is held constant at 30 kg/h, resulting in a mean mixture bulk velocity of $u_{\mathrm{bulk}} = 18\,\mathrm{m/s}$. The three injection profiles shown in Fig. 3a are applied to the reactive measurements for 150 cycles with a firing frequency of 5 Hz. Figure 4 shows sample pressure histories of the five distributed pressure sensors for a single cycle. The ignition begins approximately 72 ms after the start of the fuel injection. At peak **1** in Fig. 4 the maximum pressure rise is reached and then starts decreasing due to expansion of the burned gas in upstream and downstream directions. Pressure waves that travel upstream are reflected at the acoustically closed inlet and result in a sharp rise in pressure (**2**). Pressure waves propagating downstream are reflected at the tube outlet as an expansion wave (**3**) that travels upstream. This expansion wave can be used to support the refilling of the combustor.

For each cycle, the maximum relative pressure increase Δp_{max} is calculated as the difference between the mean maximum pressure in peak **1** and the pressure before ignition. The expression 'ignition time' is introduced and is calculated from the pressure data τ_{p} as the time delay between the starting point of the injection until the first increase in pressure exceeding a threshold of 0.03 bar. A similar τ_{i} is derived from the ionization probe data as labeled in Fig. 4. The difference between these two ignition times is labeled $\Delta\tau_{\mathrm{ip}}$. 'Ignition delay time' is ambiguous due to the long injection period.

The amplitude of the pressure rise is plotted against the coherency of the ignition ($\Delta\tau_{\mathrm{ip}}$) in Fig. 5 for the three injection profiles. There is quite a lot of cycle-to-cycle variance for each specific fuel profile. However, there is a notable shift towards higher pressure amplitudes for lower $\Delta\tau_{\mathrm{ip}}$. Also, the three profiles tend to cluster throughout this graph, indicating that the Λ-curve tends towards smaller $\Delta\tau_{\mathrm{ip}}$ while the V-curve is less homogeneous. The $\sqcap$-curve falls generally in between. Low $\Delta\tau_{\mathrm{ip}}$ indicates a more quasi-simultaneous detection of ignition and pressure rise, whereas higher $\Delta\tau_{\mathrm{ip}}$ implies a later or less homogeneous ignition compared. With decreasing $\Delta\tau_{\mathrm{ip}}$, the resulting pressure amplitude is increasing significantly. According to Oppenheim [16], two characteristic modes of ignition can be generally observed: (i) mild ignition and (ii) strong ignition. The latter case can be described as a reaction front with a detonation-like structure characterized by a sharp increase in pressure. A mild ignition appears due to multiple autoignition sources that propagate chaotically and individually. All observed ignitions that are shown in Fig. 5 can be categorized as mild ignitions differing in the number of autoignition sources. This conclusion is based on the comparison of the gradual pressure increase ($t \approx 73$ ms in Fig. 4) subsequent to the autoignition when comparing to the steep increase of the reflected wave ($t \approx 76$ ms in Fig. 4) as suggested by Bartenev and Gelfand [6]. However, comparing **regime 1** to **regime 2** shows that under certain conditions, multiple autoignition sources can initiate a reaction front that is more likely to couple with the pressure rise resulting in a greater pressure.

To characterize the pressure response within the com-

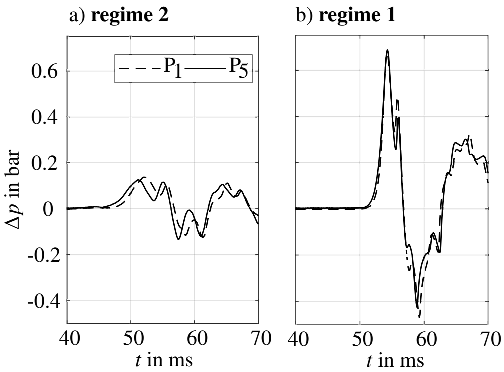

Figure 6: Dominant POD mode calculated from pressure data for **regime 2** (a) and **regime 1** (b).

bustor, proper orthogonal decomposition (POD) was applied to the pressure data of 50 cycles for both regions identified in Fig. 5. The dominant POD modes of the pressure histories of sensors P_1 and P_5 are shown in Fig. 6.

Figure 6a shows a much weaker pressure wave traveling upstream the combustor with the speed of sound detected by sensor P_5 and later by sensor P_1 respectively. The propagation velocity of the ignition front is slower such that limited coupling between the pressure wave and heat release occurs. Figure 6b shows a nearly simultaneous detection of the pressure increase by sensors P_1 and P_5. A gradual, non-sharp (compared to a shock wave) rise in pressure is noticeable. The period of elevated pressure was calculated to a mean value of 7.4 and 6.7 ms for V-curve and Λ-curve respectively with a standard deviation of this period of 1.1 ms for both injection profiles. The prolonged duration of pressure increase results from a wider spatial distribution of the ignition event for the V-curve whereas a more homogeneous ignition for the Λ-curve results in a more distinct pressure rise. Due to the higher pressure amplitude in **regime 1**, the expansion wave that arises from the reflection at the tube outlet is more pronounced resulting in a lower pressure for $57\,\mathrm{ms} < t < 62\,\mathrm{ms}$. The period of low pressure was calculated to be 5.5 and 5.8 ms with a standard deviation of 0.3 ms. These calculations indicate that there is little correlation between the duration of the high pressure and the time span of low pressure. Hence, this low pressure region is caused by reflection of pressure waves at the acoustically open end of the combustor and is therefore a function of acoustic time scales only, which do not change for the conducted measurements.

Based on the observed variations in pressure and ionization probe histories for the ignition events as shown in Fig. 5, the homogeneity in autoignition was found to be primarily responsible for larger pressure rises. Because the specific fuel injection profiles used in this study are not optimized to achieve consistent, homogeneous autoignition, they therefore show significant variation in the likelihood of a uniform autoignition which results in the broadened distributions shown above.

To further explore the ignition process, the setup with an optical access as shown in Fig. 2b is used to measure OH^* intensity and the pressure simultaneously. Figure 7 shows x-t-diagrams of the OH^* intensity for the downstream part of section 1 and sections 2 and 3 of the optical setup for three sample shots. Every time step in the x-t-diagrams represents an average OH^* intensity for all pixels of a single image at the respective axial position. 649 snapshots are aligned for each figure. The vertical shadows in the images correspond to the combustor supports and the pressure traces (P_2 and P_3) at these locations are overlaid. The white line represents the ignition time τ_o for each axial position that is defined by the OH^* intensity exceeding a threshold of 0.079. The temporal position is aligned to the earliest ignition point within the frame. Figures 7a and b show two different cycles for the Λ-curve while the Fig. 7c on the right results from measurements with the V-curve. These three cycles have been selected to be representative of the various visible ignition events observed for many cycles. Lastly, it is important to recall, that there is a constant bulk flow in the positive x-direction before ignition.

A uniform, highly distributed ignition front with multiple points of ignition is shown in Fig. 7a. Compared with the other examples, the region after ignition shows the highest OH^* intensity. Furthermore, the largest amplitude in the pressure signals are observed. The majority of the high intensity OH^* occurs within a period of about $\Delta t = 2\,\mathrm{ms}$. There also appears to be a propagation of the gas in the upstream direction for $x < 200\,\mathrm{mm}$ and in downstream direction for $x > 200\,\mathrm{mm}$ respectively. The distributed ignition results in an aerodynamic confinement, which serves to increase the pressure more than in the other examples. As the products expand, the pressure falls and eventually reaches a local minimum for $\Delta t \approx 3\,\mathrm{ms}$. As previously mentioned, the pressure wave propagating upstream is reflected at the tube inlet and propagates downstream which is visible as a second pressure peak in Fig. 7a at $\Delta t \approx 3.5\,\mathrm{ms}$. At the acoustically open tube outlet, this pressure wave is reflected as an expansion wave that causes a low pressure region for $\Delta t > 5\,\mathrm{ms}$.

The ignition front in Fig. 7b is less uniform, and instead propagates primarily from a single ignition point at $x \approx 100\,\mathrm{mm}$. From this source, the ignition front propagates in both axial directions. The propagation

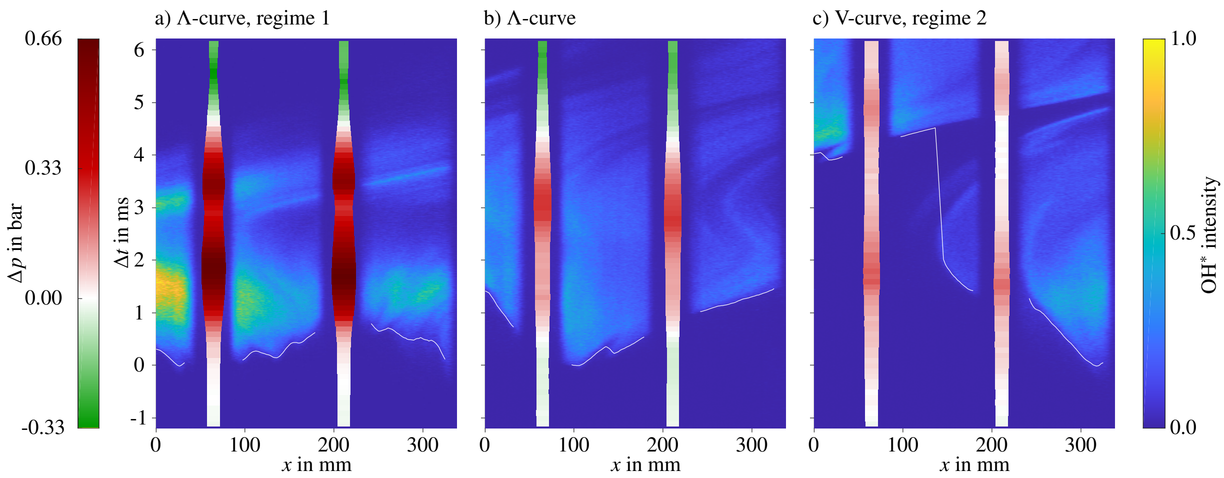

Figure 7: x-t-diagrams for OH* intensity and pressure histories for P_2 and P_3 for three example shots. The spatial range of each figure covers the downstream part section 1 and the sections 2 and 3 of the optical accessible combustor (Fig. 2b). The white line represents the spatial distribution of the ignition time τ_o that is defined by the OH* intensity. The temporal positions of the three figures are adjusted by $\Delta t = t - \tau_{o,min}$.

velocity in the lab frame reference can be estimated using the slopes of the fronts in the x-t-diagram as $u_{a,US} \approx -68$ m/s and $u_{a,DS} \approx 112$ m/s for upstream (US) and downstream (DS) direction, respectively. Accounting for the bulk flow velocity of $u_{bulk} \approx 18$ m/s, a nearly constant propagation velocity of $u_a \approx -86$ and 94 m/s can be found, which suggests that the propagation of the ignition front in Fig. 7b is a propagating turbulent flame, rather than an autoignition front.

Figure 7c shows the distribution of OH* intensity for a measurement with the V-curve. The first ignition point occurs close to or just outside of the image frame. Compared with the first two examples, the autoignition occurs much further downstream in the combustor due to the richer mixture at the beginning of the injection. Subsequently, a deflagration propagates upstream in the combustor at $u_{a,US} \approx -70$ m/s in the lab frame reference. Simultaneously, a weaker pressure wave can be seen in the pressure histories travelling at the speed of sound. At $\Delta t = 4$ ms, a second deflagration front is propagating downstream in the combustor which indicates a second autoignition event has occurred further upstream of the combustor (presumably also due to the second high equivalence ratio region at the end of the V-curve injection profile). In this case, the reduced aerodynamic confinement due to multiple, separated ignition points results in the smallest increase in pressure of the three examples. The acceleration of the flow due to the upstream ignition event results in the two propagating fronts, and the curved trajectories in the fixed laboratory frame.

From Fig. 7a to 7c, the inhomogeneity of the ignition front τ_o increases, which can be expressed by an increase of the standard deviation of the ignition time std (τ_o). This increase in std (τ_o) corresponds to a decrease in the maximum pressure amplitude Δp_{max}. Simultaneously, a decrease in the OH* intensity and the amplitude of the subsequent low pressure region Δp_{min} is visible.

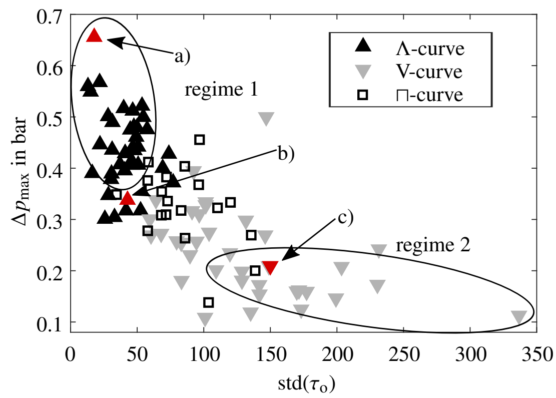

Figure 8: Pressure amplitude over standard deviation of the ignition time std(τ_o) plotted for V-curve, Λ-curve and ⊓-curve. The highlighted markers represent the three shots shown in Fig. 7.

Figure 8 shows Δp_{max} as a function of std (τ_o) for all measured cycles with the three injection profiles. The three examples presented in Fig. 7 are highlighted. Shots with high variance in the ignition front (large std (τ_o)) correspond to a lower pressure rise than those with more uniform ignition. The time delay between detecting a pressure rise and a combustion event (from either an ionization probe or OH*), as shown in

Figs. 5 and 8, shows a consistent trend. When the time delay between the pressure rise and the combustion event is coupled (as in **regime 1**), the distributed heat release results in a greater pressure rise due to the aerodynamic confinement compared with the uncoupled **regime 2**. Achieving this type of autoignition event consistently and routinely is the objective of utilizing the SEC for pressure gain combustion. Towards this aim, on-going work is focused on tailoring the specific injection profile to maximize this pressure rise as well as the consistency in autoignition homogeneity.

4. Conclusion and Outlook

This work presented a novel combustion rig equipped with a controllable reactant injection system designed to deliver a prescribed, stratified charge of autoignitable mixture. The reproducibility of the system for three injection profiles was demonstrated. Then, the correlation between pressure rise and distribution of ignition events was shown.

It was observed that a temporal decoupling between pressure rise and flame detection by ion probe was associated with a lower overall pressure rise. Observing the ignition process for different ignition regimes, broadly classified as **regimes 1** and **2**, supported the conclusion that a distributed, uniform autoignition event results in a greater overall pressure rise. This work has shown that these phenomena are repeatable and measurable, which is an important requirement for the use of a shockless explosion combustor as a pressure gain combustion device, where the concept of aerodynamic confinement during autoignition is comparable with constant volume combustion.

Using three arbitrary injection profiles in this work demonstrated a variety of ignition distributions. This work therefore serves as a starting point for the refinement of injection profiles in order to maximize the pressure rise and minimize the variability in ignition occurrence as well as to later implement closed-loop control of the injection scheme. Despite the variability in the profiles studied here, it is already seen that a significant portion of ignition events follow the process in **regime 1** and that the injection profile is very controllable. Both are important results for progressing the controlled autoignition and studying these combustion events in stratified mixtures.

Acknowledgments

The authors gratefully acknowledge the support of the Deutsche Forschungsgemeinschaft (DFG) as part of Collaborative Research Center CRC 1029 "Substantial efficiency increase in gas turbines through direct use of coupled unsteady combustion and flow dynamics". The authors also wish to thank Andy Göhrs and Thorsten Dessin for their technical support.

References

[1] J. Gray, M. Lemke, J. Reiss, C. Paschereit, J. Sesterhenn, J. Moeck, A compact shock-focusing geometry for detonation initiation: experiments and adjoint-based variational data assimilation, Combust. Flame 183 (2017) 144–156.

[2] R. Bluemner, M. D. Bohon, C. O. Paschereit, E. J. Gutmark, Single and counter-rotating wave modes in an RDC, AIAA Paper 2018-1608.

[3] B. C. Bobusch, P. Berndt, C. O. Paschereit, R. Klein, Shockless explosion combustion: An innovative way of efficient constant volume combustion in gas turbines, Combust. Sci. Technol. 186 (10-11) (2014) 1680–1689.

[4] Y. B. Zeldovich, Regime classification of an exothermic reaction with nonuniform initial conditions, Combust. Flame 39 (2) (1980) 211–214.

[5] X. Gu, D. Emerson, D. Bradley, Modes of reaction front propagation from hot spots, Combust. Flame 133 (1-2) (2003) 63–74.

[6] A. Bartenev, B. Gelfand, Spontaneous initiation of detonations, Prog. Energ. Combust. 26 (1) (2000) 29–55.

[7] F. Zhao, T. N. Asmus, D. N. Assanis, J. E. Dec, J. A. Eng, P. M. Najt, Homogeneous charge compression ignition (hcci) engines, Tech. rep., SAE Technical Paper (2003).

[8] J. Eng, Characterization of pressure waves in hcci combustion, Tech. rep., SAE Technical Paper (2002).

[9] B. C. Bobusch, Fluidic devices for realizing the shockless explosion combustion process, Ph.D. thesis, TU Berlin (2015).

[10] T. G. Reichel, J.-S. Schäpel, B. C. Bobusch, R. Klein, R. King, C. O. Paschereit, Shockless explosion combustion: Experimental investigation of a new approximate constant volume combustion process, J. Eng. Gas Turb. Power 139 (2) (2017) 021504.

[11] F. C. Yücel, F. Völzke, C. O. Paschereit, Effect of the switching times on the operating behavior of a shockless explosion combustor, in: Active Flow and Combustion Control 2018, Springer, 2019, pp. 121–134.

[12] H. Li, S. D. Wehe, K. R. McManus, Real-time equivalence ratio measurements in gas turbine combustors with a near-infrared diode laser sensor, P. Combust. Inst. 33 (1) (2011) 717–724.

[13] J.-S. Schäpel, R. King, F. Yücel, F. Völzke, C. O. Paschereit, R. Klein, Fuel injection control for a valve array in a shockless explosion combustor, in: ASME Turbo Expo 2018: Turbomachinery Technical Conference and Exposition, American Society of Mechanical Engineers Digital Collection, 2018.

[14] U. Burke, K. P. Somers, P. O'Toole, C. M. Zinner, N. Marquet, G. Bourque, E. L. Petersen, W. K. Metcalfe, Z. Serinyel, H. J. Curran, An ignition delay and kinetic modeling study of methane, dimethyl ether, and their mixtures at high pressures, Combust. Flame 162 (2) (2015) 315–330.

[15] D. G. Goodwin, R. L. Speth, H. K. Moffat, B. W. Weber, Cantera: An object-oriented software toolkit for chemical kinetics, thermodynamics, and transport processes, https://www.cantera.org, version 2.4.0 (2018). doi:10.5281/zenodo.1174508.

[16] A. K. Oppenheim, Dynamic features of combustion, Philos. T. R. Soc. A 315 (1534) (1985) 471–508.